Depressed Phase Transition in Solution-Grown VO_2 Nanostructures

By Luisa Whittaker,[1] Cherno Jaye,[2] Zugen Fu,[2] Daniel A. Fischer,[2] and Sarbajit Banerjee[1]*

1. Department of Chemistry, University at Buffalo, State University of New York, Buffalo, NY 14260;

E-mail: sb244@buffalo.edu

2.   Materials Science and Engineering Laboratory, National Institute of Standards and Technology,

Gaithersburg, MD 20899

ABSTRACT

The first-order metal—insulator phase transition in VO_2 is characterized by an ultrafast several orders of magnitude change in electrical conductivity and optical transmittance, which makes this material an attractive candidate for the fabrication of optical limiting elements, thermochromic coatings, and Mott field-effect transistors. Here, we demonstrate that the phase transition temperature and hysteresis can be tuned by scaling VO_2 to nanoscale dimensions. A simple hydrothermal protocol yields anisotropic free-standing single-crystalline VO_2 nanostructures with a phase-transition temperature depressed to as low as 32°C from 67°C in the bulk. The observations here point to the importance of carefully controlling the stochiometry and dimensions of VO_2 nanostructures to tune the phase transition in this system.

KEYWORDS

Vanadium oxide, metal-insulator phase transition, monoclinic, tetragonal

INTRODUCTION

Nanoscale materials with at least one dimension smaller than 100 nm exhibit remarkable properties that are often not observed for their bulk counterparts.[1, 2] The dramatic modifications to

1

physical and chemical properties at nanoscale dimensions originates from quantum confinement effects, fairly subtle structural changes, or the increased contributions from atoms residing on the surface.[3, 4] Much effort over the last decade has focused on elucidation of finite size effects in semiconductors;[5] indeed, II—VI chalcogenide quantum dots represent a particularly well-developed example of the remarkable applications possible upon scaling materials to nanoscale dimensions.[6] The role of finite size in modifying the properties of transition metal oxides has only recently started to attract attention.[7-9] Vanadium oxides represent particularly attractive systems for such investigations because of their tremendous structural diversity arising from the facile accessibility of different vanadium oxidation states and their high tolerance for point defects.[7, 10-12] Apart from the stoichiometric phases VO, V_2O_3, VO_2, and V_2O_5, a closely related set of structures with the stoichiometry V_nO_{2n-1} and V_nO_{2n+1} are known that are able to accommodate point defects via means such as the formation of crystallographic shear structures. Arguably the two most notable compounds in this series have been V_2O_3 and VO_2, which have long been textbook examples of systems exhibiting well-defined metal—insulator phase transitions with changes in electrical conductivity ranging up to five orders of magnitude.[13-15] VO_2, in particular, has attracted tremendous interest over almost half a century and is a benchmark problem in solid-state chemistry because of its near-room temperature metal—insulator phase transition at ~67°C. The ultrafast first-order phase transition in VO_2 is also accompanied by a dramatic modification of the optical absorbance; below the phase-transition temperature VO_2 is a narrow bandgap semiconductor (bandgap of ~0.7 eV) and is transparent over the infrared region of the electromagnetic spectrum, whereas the higher temperature metallic phase of VO_2 is opaque at most frequencies. These remarkable coupled orders-of-magnitude near-room-temperature changes in optical and electrical properties make this material very attractive for applications such as Mott field-effect transistors, switching devices, optical waveguides, optical limiting elements, sensing components, and thermochromic coatings.[10, 13, 16-18]

Interestingly, despite the strong theoretical and experimental interest in this material, a fundamental understanding of the origin of the phase transition in VO_2 remains elusive.[19-21] A rather vigorous and longstanding debate in the literature focuses on the relative importance of electron-lattice coupling and correlated electrons in triggering the phase transition. Indeed, this phase transition has been variously ascribed to Mott-Hubbard or Peierls lattice distortion types (or even a mix of both!).[14, 19, 20, 22-24] For instance, a recent cluster dynamical mean field theory study asserts that singlet pairing and strong Coulomb interactions are both required to open up a gap in the insulating phase upon cooling to the metal—insulator phase transition temperature.[25] This model emphasizes a large redistribution of electron occupancies in favor of a non-bonding orbital (the $d_\parallel$ band) derived from the hybridization of V $3d_{xy}$ states with O $2p_z$ levels and has drawn extensive support from recent photoemission and X-ray absorption studies.[26, 27]

According to the Peierls structural phase transition model, a small structural change from an insulating antiferromagnetic monoclinic phase to a metallic paramagnetic tetragonal phase accompanies this phase transition with strong electron—lattice coupling contributing extensively to the observed changes in conductivity and optical transmittance.[15] **Figure 1** shows the crystal structures of the (high temperature) tetragonal and (low temperature) monoclinic polymorphs of VO_2. The tetragonal structure formed above the metal—insulator phase transition temperature corresponds to a relatively more isotropic arrangement and is based on adjacent [VO_6] octahedra sharing edges along the c-axis to form a hexagonal close-packed lattice with considerable V—V overlap.[15] In contrast, the unit cell is doubled in the insulating monoclinic phase because of a small distortion of the [VO_6] octahedra yielding alternate long and short V—V bonds with reduction in symmetry to C_{2h} point group.[15, 28] Notably, other theoretical models attempting to explain the metal—insulator phase transition in VO_2 have emphasized the importance of electron—electron correlations.[19] This general view has been bolstered by recent work by Kim and co-workers, which very elegantly illustrates that the metal—insulator phase transition in

VO$_2$ can be induced by hole doping either via photoassisted hole excitation or by the application of an electric field without the need for a structural phase transition.[23, 24, 29] These authors have demonstrated the existence of a non-equilibrium metallic monoclinic phase that persists between the metal—insulator phase transition temperature and the monoclinic→rutile structural phase transition. These studies particularly emphasize the hole-driven nature of this Mott transition. The recent demonstration of this electric-field induced transition and reports of the ultrafast nature of this phase transition[20, 23, 29-31] have lead to renewed interest in VO$_2$ for integration in Mott field-effect transistors and switching elements.[22] For integration in room-temperature devices and coatings, regardless of the structural/electronic origin of the phase transition, there is considerable interest in being able to shift the metal—insulator phase transition in VO$_2$ to lower temperatures. Indeed, the phase transition temperature in VO$_2$ is remarkably sensitive to the presence of dopants and strain. Some recent findings by Feldman, Lopez, and co-workers suggest the intriguing possibility of tuning the phase transition temperature and hysteresis in VO$_2$ by scaling these systems to nanoscale dimensions. In a series of articles, these authors have indeed demonstrated a strong finite-size effect on the phase transition temperature and hysteresis in VO$_2$ nanostructures prepared by top-down methods such as laser ablation or ion implantation in SiO$_2$ matrices.[11, 17, 18] These authors have demonstrated that significant undercooling is required to induce the phase transition in their ion-implanted VO$_2$ nanostructures. Invoking a Martensitic-like behavior, they postulate that the elimination of defects that can serve as nucleation sites for the phase transition leads to the need for a stronger driving force (lower/higher temperature). Remarkably, however, for VO$_2$ nanostructures prepared by bottom-up methods such as chemical vapor deposition and especially by solution-chemistry approaches, the metal—insulator phase transition appears to be very significantly smeared out or even completely absent, making it difficult to understand the influence of finite size on the structural/electronic phase transition in these systems.[32-35] The absence or diminished magnitude of the characteristic metal—insulator phase transition has been variously attributed to local deviations in

oxygen stoichiometries or strain imposed on nanostructures as a result of adhesion to underlying substrates.[32, 33] Indeed, it is well known that the metal—insulator transition in VO_2 is very sensitive to the stoichiometry and crystallinity of the measured systems.[32, 36, 37] In a recent investigation, Ramanathan and co-workers have carried out detailed measurements to correlate electron transport data directly to the band structure derived from near-edge X-ray absorption fine structure spectroscopy (NEXAFS) measurements for VO_2 thin films fabricated by reactive sputtering of a V target.[38] These authors have found that the metal—insulator phase transition and the electron correlations involved in the phase transition depend sensitively on the oxygen stoichiometry—a change in the anion stoichiometry by a few percent can lead to several orders of magnitude difference in the phase transition behavior. These findings underline the need to develop synthetic approaches that can yield free-standing nanostructures with careful control of these parameters. Here, we provide clear evidence for highly depressed phase transitions in anisotropic free-standing VO_2 nanostructures prepared by the hydrothermal cleavage of bulk VO_2 in the presence of aliphatic alcohols.

While several approaches for the fabrication of VO_2 nanostructures have been reported previously in the literature including, rf sputtering, hydrothermal syntheses,[34, 35, 39] controlled oxidation and sputtering, and vapor transport onto Si_3N_4 substrates,[32, 40] evidence for well-defined phase transitions has remained elusive. Here, we demonstrate well-defined structural phase transitions in VO_2 nanowires, nanorods, and nanosheets grown from solution that are significantly depressed from the bulk VO_2 phase transition temperature of ~67°C to temperatures as low as 32 °C.

EXPERIMENTAL

Synthesis: VO_2 nanostructures were synthesized solvothermally by the hydration/cleavage/exfoliation of bulk V_2O_4 (Sigma Aldrich, >99.5%) using Parr acid digestion bombs. Aliphatic alcohols used as structure-directing agents were obtained from Fisher. Deionized water from a Barnstead International

NANOpure Diamond ultrapure water system (ρ = 18.2 MΩ/cm) was used to prepare all aqueous solutions. In a typical reaction, 1.8 mmol of V_2O_4 was mixed with 1 mL of the structure-directing species and 16 mL of deionized water. The resulting mixture was placed in a 23 mL Teflon cup that was then heated in a sealed autoclave at 210°C for varying times (3—7 days). The precipitate obtained upon cooling to room temperature was washed with copious amounts of deionized water and acetone and then dried at ambient temperature.

Characterization: The morphologies of the resulting products were examined by scanning electron microscopy (SEM, JSM-5610LV operated at 20 kV) and transmission electron microscopy (TEM, JEOL 2010 operated at 200 kV). For TEM observations, the nanostructures were dispersed in 2-propanol solution and drop-cast onto 300 mesh carbon-coated Cu grids. Phase identification was performed using X-ray diffraction (XRD, Siemens D-500 with Cu Kα radiation, λ = 1.5418 Å). Differential scanning calorimetry (DSC Q 200 TA Instruments) measurements under a flowing gaseous nitrogen atmosphere over a temperature range from 20 to 150°C were used to study the phase transitions in the as-prepared nanostructures over repeated heating/cooling cycles. The electronic structure of the VO_2 nanostructures was studied by V L-edge and O K-edge NEXAFS measurements performed on the National Institute of Standards and Technology beamline U7A at the National Synchrotron Light Source of Brookhaven National Laboratory. A toroidal mirror spherical grating monochromator using a 1200 lines/mm grating with a nominal energy resolution of ~0.1 eV was used for these measurements. The spectra were acquired in partial electron yield mode using a channeltron electron multiplier located near the sample using the detector at an entrance grid bias of −200 V to enhance surface sensitivity. A charge compensation gun was used to avoid sample charging. A vanadium mesh was used as a reference standard for calibration of the energy scale for each spectrum. To eliminate the effects of incident beam intensity fluctuations and monochromator absorption features, the partial electron yield signals were normalized using the drain current of a freshly evaporated gold mesh with 90% transmittance located

along the path of the incident X-rays. For heating experiments, the samples were mounted onto a homemade holder constructed using tantalum foil with a welded thermocouple. All data here have been acquired at magic angle ($\theta = 54.7°$) incidence of the X-ray beam. Pre- and post-edge normalization of the data were performed using the Athena suite of programs.

Results and Discussion

Figure 2 shows SEM images of VO_2 nanostructures obtained upon the cleavage/exfoliation of bulk VO_2 using 1,3-butanediol, 2-propanol, and methanol as structure-directing agents. Anisotropic monoclinic VO_2 nanostructures have been obtained for all the alcohols listed in Table 1. Unlike V_2O_5, V_6O_{13}, and several hydrated vanadium oxides, monoclinic VO_2 does not form a layered structure.[15] However, Wei and co-workers have demonstrated the preparation of hydrated $V_2O_4 \cdot 0.25H_2O$ nanowires with a layered structure upon the hydrothermal treatment of monoclinic VO_2.[41] Indeed, several layered hydrated structures of V_2O_4 are known with water molecules residing in the interlayer spaces between [VO_5] square pyramids. The addition of simple aliphatic alcohols to the hydrothermal protocol profoundly affects the morphology, crystal structure, and properties of the obtained structures. Figure 2 illustrates the different morphologies obtained upon the hydrothermal treatment of bulk (micrometer-sized) V_2O_4 powder with a closely related series of alcohols. **Figure 2** also shows transmission electron microscopy images that further confirm the formation of ultra-thin VO_2 nanostructures with smooth edges. **Figure 3** illustrates powder XRD patterns acquired for these three samples. The XRD patterns can be indexed to monoclinic VO_2(M) (Joint Committee on Powder Diffraction Standards (JCPDS) No. 043-1051). The strong intensity of the {011} reflections points to the strongly preferential growth direction of these structures, as has also been noted previously for VO_2 nanowires prepared at high temperatures by vapor transport.[40] Notably, upon hydrothermal reaction for 7 days, 1,3-butanediol yields relatively short nanowires with clearly faceted rectangular cross-sections. The nanowires vary in length

from several hundred nanometers to about 10 μm. In contrast after reaction for 7 days, methanol affords relatively longer and thinner "straw-like" nanowires with faceted ends, as evidenced in Figure 2C. The hydrothermal reaction of bulk V_2O_4 with these alcohols for shorter periods of time on the order of 72 h does not yield uniform nanowires although irregularly shaped microstructures and some nanoparticulate material is observed. In contrast, 2-propanol yields nanosheet morphologies that can be up to several tens of micrometers long after hydrothermal reaction for 72 h. These nanosheets are relatively thin with thicknesses typically less than 50 nm. Longer reactions times appear to cause disintegration of these nanowires to more irregular morphologies.

Analogous to the formation of nanowires from $V_2O_4 \cdot 0.25H_2O$ and other layered structures, a hydration—exfoliation—splitting mechanism is likely to be involved in the formation of the nanowires.[41] According to this model, bulk V_2O_4 is hydrated to form a layered compound such as $V_2O_4 \cdot 0.5H_2O$ wherein water molecules reside in the interstices between layers of [VO_5] square pyramids.[41] Hagrman et al. have detailed the crystal structure of a hydrated VO_2 polymorph with water molecules intercalated in this fashion.[43] The intercalation of water as well as alcohol molecules in our syntheses eventually weakens the attraction between the layers and results in the cleavage and exfoliation of the hydrated layered structures into nanosheets. The nanosheets with adsorbed alcohols have been theoretically predicted to have a significant amount of built-in stress, which causes them to split or deform to yield different morphologies such as the nanoribbons and faceted nanowires obtained here.[44] The driving force for the deformation/splitting of the nanosheets is thought to be the lowering of energy upon relieving the tension intrinsic to the exfoliated sheets. Different from Zhou et al.,[41] the addition of alcohols that have a higher affinity for binding V relative to H_2O yields monoclinic VO_2 nanostructures rather than the hydrated $V_2O_4 \cdot 0.25H_2O$ nanosheets reported previously in the literature.

Figure 4 shows DSC data acquired for the VO_2 nanostructures. The structural phase transition in VO_2 is first-order in nature and includes a substantial entropy component that has been estimated to range from 12.6—13.8 J mol^{-1} K^{-1}.[45] Two major contributions to the latent heat at the phase transition arise from the lattice distortion and the change in conduction electrons because of the discontinuity in the carrier density.[46] Thermal analysis studies in the literature show well-defined and reproducible peaks in plots of heat capacity versus temperature at ~67°C for bulk monoclinic VO_2 samples prepared at high temperatures.[47] No such exothermic/endothermic peaks are observed for a closely related metastable monoclinic $VO_2(B)$ phase that is often obtained under hydrothermal conditions. Consistent with these observations, annealed (micrometer-sized) bulk VO_2 powder shows a well-defined phase transition at ~67°C in the heating cycle and at ~60—64°C in the cooling cycle. In contrast, the hydrothermally prepared nanostructured monoclinic VO_2 samples show starkly different thermal behavior. For VO_2 nanowire samples prepared using 1,3-butanediol to cleave and exfoliate bulk VO_2 for 7 days, the phase transition is shifted down to ~60°C during the heating cycle and to as low as 32°C during the cooling cycle. The peaks characteristic of the phase transition are also significantly broadened, which may be a result of the polydispersity in nanostructure size in the samples. Table 1 summarizes the positions of the observed DSC peaks during the heating/cooling cycles for samples prepared using different aliphatic alcohols as structure-directing agents. The nanosheet samples prepared using methanol (after a reaction time of 3 days) show peaks attributable to the structural phase transition at ~62 and ~37°C, respectively, during the heating and cooling cycles. Notably, the DSC peaks corresponding to the monoclinic→tetragonal phase transition are shifted to higher temperatures relative to the bulk during the heating cycle for the straw-like nanowires prepared using methanol as the structure-directing agent. The thermal analysis results are found to be eminently reproducible for different samples. Over different heating/cooling cycles of the same sample, there are variations of less <2°C in the DSC peaks. Since the nanostructures are heated only to ~150°C in these measurements, no sintering of the structures is

expected or observed. A hysteresis in the phase transition between cooling and heating cycles is characteristic of the first-order structural transition in VO_2. Notably, the hysteresis loop is observed to be much wider for all the samples upon scaling to nanoscale dimensions. This increased hysteresis is consistent with observations from Feldman and co-workers for VO_2 nanostructures grown by top-down methods such as ion implantation.[17] Consistent with the observed depression in the phase transition temperature being a finite size effect, Table 1 illustrates that increasing the reaction time from 3 to 7 days leads to increased depression of the phase transition temperature for all the structure-directing agents screened in our experiments. An increased hydrothermal reaction time corresponds to greater splitting of the nanosheets and nanowires to smaller dimensions, which clearly leads to further depression of the phase transition temperature. Notably, this trend still holds true even for the hydrothermal reaction of V_2O_4 with 2-propanol where the clean nanosheet samples observed after 3 days are shredded to smaller irregular shaped fragments after hydrothermal reaction for 7 days. The phase transition temperature is decreased by ~10°C from 57°C to 47°C during the cooling cycle upon increasing the hydrothermal treatment time.

Further characterization of the electronic structure and phase transition behavior of the obtained VO_2 nanostructures comes from soft X-ray absorption spectroscopy measurements (**Figure 5**). NEXAFS is a powerful element-specific tool for probing the frontier orbitals of VO_2 based on the excitation of core hole states to partially filled and empty states.[48] Given the dipole selection rules for NEXAFS spectroscopy, $\Delta l = \pm 1$ with changes in spin disallowed, the V L-edge NEXAFS spectra represent the *d*-projected unoccupied density of states and the O K-edge spectra represent the *p*-projected unoccupied density of states of the valence levels.[38, 49, 50] The strong hybridization of the O 2*p* levels with the finely structured V 3*d* levels makes NEXAFS an especially powerful probe of bonding and electronic structure in VO_2.[26, 27, 50] Figure 5 compares V L-edge and O K-edge spectra acquired for VO_2 nanostructures and bulk VO_2. The V L-edge region shows two peaks at 517 and 524 eV that can be attributed to V2$p_{3/2}$→3d

and V $2p_{1/2} \rightarrow 3d$ transitions, respectively. Notably, the peak positions of the V L-edge peaks are known to shift by about 0.7 eV for each oxidation state.[51] The similarity in the lineshapes and peak positions (within ±0.2 eV) observed here confirms the retention of the V^{4+} oxidation state in the nanostructures upon hydrothermal treatment. Indeed, the spin-orbit splitting of the $2p$ levels is ca. 6.6 eV for the VO_2 nanostructures, exactly the same value derived from XAS studies of VO_2 single crystals. A shoulder to the V L_{III} peak is observed at ~515 eV and is suggestive of the excellent crystallinity of the samples.[49] This feature is more pronounced in single crystals of VO_2 but is absent in spectra acquired for VO_2 powders or polycrystalline thin films on Si_3N_4.[49, 50] Ruzmetov et al. have observed that the sharpness of this feature is strongly correlated to the texture of their polycrystalline VO_2 films—distinctive satellite peaks are observed only for films showing excellent crystallinity with a relatively large grain size.[50] The observation of pronounced shoulders especially for the nanosheet and faceted nanowire samples prepared using 2-propanol and 1,3 butanediol, respectively, under magic angle incidence of the X-ray beam attest to the excellent crystallinity of the samples (and perhaps also to the presence of some preferred orientation). Based on Goodenough's description of the band structure of VO_2,[15] the V L-edge absorption for the monoclinic insulating phase of VO_2 primarily describes transitions into $d_\parallel$ non-bonding levels, whereas the O K-edge spectra describe transitions into π^*, σ^*, and $d_\parallel$ levels. The dipole selection rules for NEXAFS imply that the O K-edge is characterized by transitions from O $1s$ core levels to states possessing O $2p$ symmetry. The O $2p$ levels are strongly hybridized with V $3d$ levels and thus the O K-edge spectral features serve as a very precise probe of these finely structured states. The approximately octahedral crystal field in VO_2 splits the V 3d levels into higher e_g and lower t_{2g} levels. In the high-temperature rutile phase with more symmetric VO_6 octahedra, the V $3d_{z2}$ and $3d_{x2-y2}$ orbitals point directly towards the oxygen ligands (along the V—O—V axes) giving rise to strongly directional σ bonding interactions accompanied by a strong splitting of the bonding/antibonding levels.[26, 50] Figure 6 illustrates the axes definitions used to describe the bonding interactions in VO_2. Of the t_{2g} set of

orbitals, the $3d_{xz}$ and $3d_{yz}$ orbitals point in between the ligands and are involved in π interactions. Since these interactions are weaker, the unfilled antibonding π^* states lie closer to the Fermi level at relatively lower energies in the conduction band (correspondingly, the filled π states lie higher in energy in the valence band). The remaining orbital from the t_{2g} set, the V $3d_{xy}$ orbital, points in between the ligands towards the nearest neighbor V atom and remains non-bonding in the high-temperature rutile phase. Figure 6 also shows a modified version of Goodenough's band structure diagram illustrating the position of the partially filled $d_\parallel$ band (overlapping with the π^* band) derived from the non-bonding V $3d_{xy}$ orbital at the Fermi level in the metallic phase.[15] The distortion of the VO_6 octahedra upon cooling to the lower symmetry monoclinic phase gives rise to alternating long and short V—V bonds (Fig. 1). The resulting dimerization of the vanadium chains along the crystallographic c axis and the twisting of the V—V axis drastically alters the band structure. As a result of this distortion and electron repulsions, the $d_\parallel$ band is split with the unoccupied part of the band being pushed past the π^* band edge in energy because of localized pairing interactions and the filled part of the $d_\parallel$ band dropping below the Fermi level as a result of singlet pairing in the dimers, thus opening up a bandgap for the insulating phase.[50] The HOMO—LUMO bandgap between this filled $d_\parallel$ band and the unfilled π^* edge has been estimated to be ~0.7 eV from photoemission spectroscopy and optical spectroscopy measurements.[50, 52] The NEXAFS spectra in the O K-edge region is characterized by two peaks that can be understood on the band structure discussion presented above: in the insulating phase the lower energy spectral feature is a convolution of transitions to π^* and $d_\parallel$ states, whereas the higher energy resonance corresponds to transitions to σ^* states. In single crystal samples, transitions to the $d_\parallel$ states have been resolved as distinctive spectral features shifted to slightly higher energies from the π^* edge at specific polarizations of the incident beam.[50] In NEXAFS spectra of powder and polycrystalline thin films of VO_2, the averaging over different orientations smears out the distinctive π^* and $d_\parallel$ features and a broad convoluted peak is observed instead.[38,49] Compared to bulk V_2O_4, the π^* peak is clearly further

broadened in the nanostructured samples. Reports in the literature point to strong variations in the relative intensities of the σ* and π* peaks.[38] The results observed here are similar to that of powders and sputtered VO_2 films with the π* peak significantly stronger in intensity.[38, 53] Ruzmetov et al. have observed increased broadening of the spectral features and greater spectral weight for the σ* peak for VO_2 films with a smaller grain size.[38, 49] Indeed, consistent with this notion, we observe relatively lower π*/σ* intensity ratios for the nanostructures and both spectral features evidence significantly increased broadening. Some of the observed broadening may originate from the greater number of $[VO_6]$ octahedra located at the nanowire/nanosheet surfaces where some distortions to bonding may be possible as a result of surface reconstruction. The weakly structured features observed above 535 eV correspond to transitions from O $1s$ states to O $2p$ states hybridized with V $4s$ and $4p$ states. The not inconsiderable spectral weight in this region attests to the strong contribution of covalency to bonding in VO_2, typical of early transition metal oxides.[53]

To probe the changes in band structure across the phase transition, V L-edge and O K-edge NEXAFS spectra have been acquired over a heating/cooling cycle for the VO_2 nanostructures showing the most pronounced depression in phase-transition temperature, samples prepared by the hydrothermal reaction of bulk VO_2 with 1,3 butanediol. Below the phase transition temperature, the low-energy peak at the O K-edge is a convolution of transitions to π* and $d_\parallel$ states as outlined above and shown schematically in **Figure 6**. However, above the phase transition temperature, the band structure is dramatically modified and transitions into the $d_\parallel$ band are no longer observed. In NEXAFS spectra of powder and polycrystalline thin film samples this implies a significant narrowing of the low-energy feature at the O K-edge.[38, 49] Indeed, **Figure 7a** shows that as the VO_2 nanowire samples are heated past 60°C, there is a pronounced narrowing of the t_{2g} peak. The spectra can be clearly divided into two distinctive sets: the full width at half maximas (FWHMs) of the t_{2g} peaks in spectra acquired at 25, 40, and 60°C are broadened by about 30% relative to that for spectra acquired at 80, 100, and 125°C. The

latter set of data show very similar lineshapes indicating that the phase transition is complete by 80°C, as also indicated by the DSC data. Remarkably, the higher energy σ* peaks derived from hybridization of O $2p$ states with V e_g orbitals shift to slightly lower energies in the high-temperature spectra. This is consistent with literature data for VO_2 single crystals and confirms that the main changes to the band structure occur at the $d_\parallel$ band and that the σ* band is only very weakly modified by the phase transition.[50]

The NEXAFS data acquired during the cooling cycle further corroborate DSC observations of the sharply depressed phase transition temperature and increased hysteresis for VO_2 nanostructures. The low-energy t_{2g} peak at the O K-edge remains consistently narrow from 125°C to 40°C and indeed only at 30°C is the peak significantly broadened as a bandgap opens up for the insulating phase and transitions to the $d_\parallel$ band are again convoluted with the π* spectral feature. These observations are consistent with the 32°C metal to insulator phase transition temperature observed in DSC measurements. A smaller effect is seen at the V L-edge. Haverkort et al. have shown that the ~515 eV satellite peak to the V L_{III} resonance is more pronounced for the insulating phase compared to the metallic phase with significantly greater dichroicity in angle-resolved measurements.[27] Indeed, for the VO_2 nanostructures a pronounced smearing of the satellite peak is noted for spectra acquired at 80, 100, and 125°C during the heating cycle evidencing the presence of the metallic phase at these temperatures. The NEXAFS data thus demonstrate that the fundamental electronic structure of VO_2 is substantiatively preserved in the VO_2 nanostructures and that the peaks observed in the DSC traces can be correlated to changes in band structure across the metal—insulator phase transition.

Depression of the phase transition in VO_2 can have three different origins: doping with another transition metal (such as Ti), strain, and scaling to nanoscale dimensions. The relatively simple synthetic process described here does not use any other transition metals and indeed XPS and EDX studies do not

reveal the presence of any such impurities. The free standing nature of the samples rules out substantive strain as the underlying origin for the strong depression in the phase transition temperature. Indeed, as Lopez et al. have observed for VO_2 nanostructures fabricated by ion implantation or other top-down approaches,[11, 17] the changes in the phase-transition temperature likely arise from the nanoscale dimensions of the VO_2 nanostructures prepared here.[11, 17, 18] It is thought that with elimination of defects due to scaling to nanoscale dimensions, significant undercooling is required to nucleate/induce the phase transition, thus leading to a much broader hysteresis. Notably, careful control of the stoichiometry is essential to observe the phase transition. As noted above, the metal—insulator phase transition is very sensitive to the oxygen stoichiometry,[37, 38] which may be the reason clear and well-defined phase transitions have not been observed for most nanostructured material reported thus far in the literature. Consistent with the close control of VO_2 stoichiometry discussed above, upon increasing the alcohol concentration by 100%, the obtained nanostructures do not yield well-defined phase transitions. This is likely a result of the partial reduction of VO_2 by the alcohol molecules locally yielding V^{3+} domains.

In summary, we report strong finite size effects on the metal—insulator phase transition in free-standing single-crystalline nanostructures of VO_2. The phase transition has been depressed to as low as 32°C in VO_2 nanostructures from the 67°C observed in the bulk. Close control of the stoichiometry finally enables the observation of finite size effects on the VO_2 phase transition in solution-grown nanostructures that have hitherto only been observed in structures prepared by top-down methods or embedded in matrices. The unprecedented depressed phase transitions observed for VO_2 nanowires paves the way for their use in optical waveguides, Mott field-effect transistors, sensing elements and as components for thermochromic coatings.

ACKNOWLEDGMENTS

FIGURE CAPTIONS

Figure 1. Monoclinic (distorted VO_6) and tetragonal (undistorted VO_6) polymorphs of vanadium (IV) oxide.

Figure 2. SEM (left) and TEM (right) images of VO_2 nanostructures prepared by the solvothermal reaction of bulk V_2O_4 with (A,B) 2-propanol for 3 days (C,D) methanol for 7 days, and (E,F) 1,3 butanediol for 7 days.

Figure 3. XRD patterns of VO_2 nanowires prepared by the hydrothermal treatment of bulk V_2O_4 with A) 2-propanol for 3 days, B) methanol for 7 days, C) 1,3 butanediol for 7 days.

Figure 4. DSC curves obtained for VO_2 nanowires prepared by the hydrothermal treatment of bulk V_2O_4 with A) 2-propanol for 3 days, B) methanol for 7 days, and C) 1,3 butanediol for 7 days compared with the DSC trace measured for D) the bulk V_2O_4 precursor.

Figure 5. V L edge ($2p_{3/2}$, $2p_{1/2}$) and O K edge (π^*, σ^*) NEXAFS data acquired at room temperature for VO_2 nanostructures prepared by hydrothermally treating bulk V_2O_4 with A) 2-propanol for 3 days, B) methanol for 7 days, and C) 1,3 butanediol for 7 days contrasted with D) the spectra acquired for the bulk V_2O_4 powder precursor.
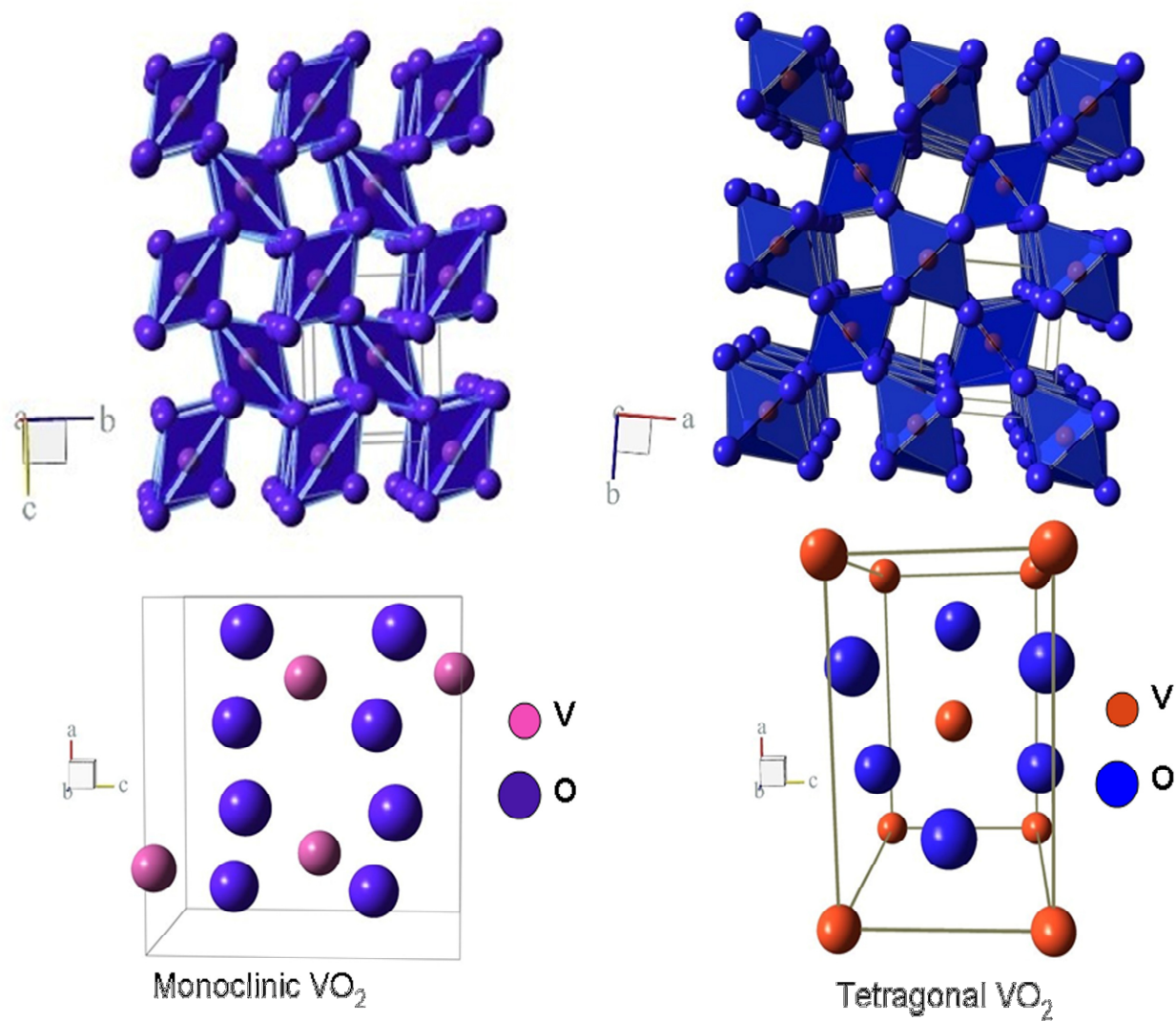
Figure 6. Molecular orbital diagram depicting the electronic structure of the two polymorphs of VO_2. The left MO diagram corresponds to the undistorted metallic phase of VO_2, whereas the diagram on the right shows the altered MO diagram upon transition to the distorted insulating phase of VO_2.[50]
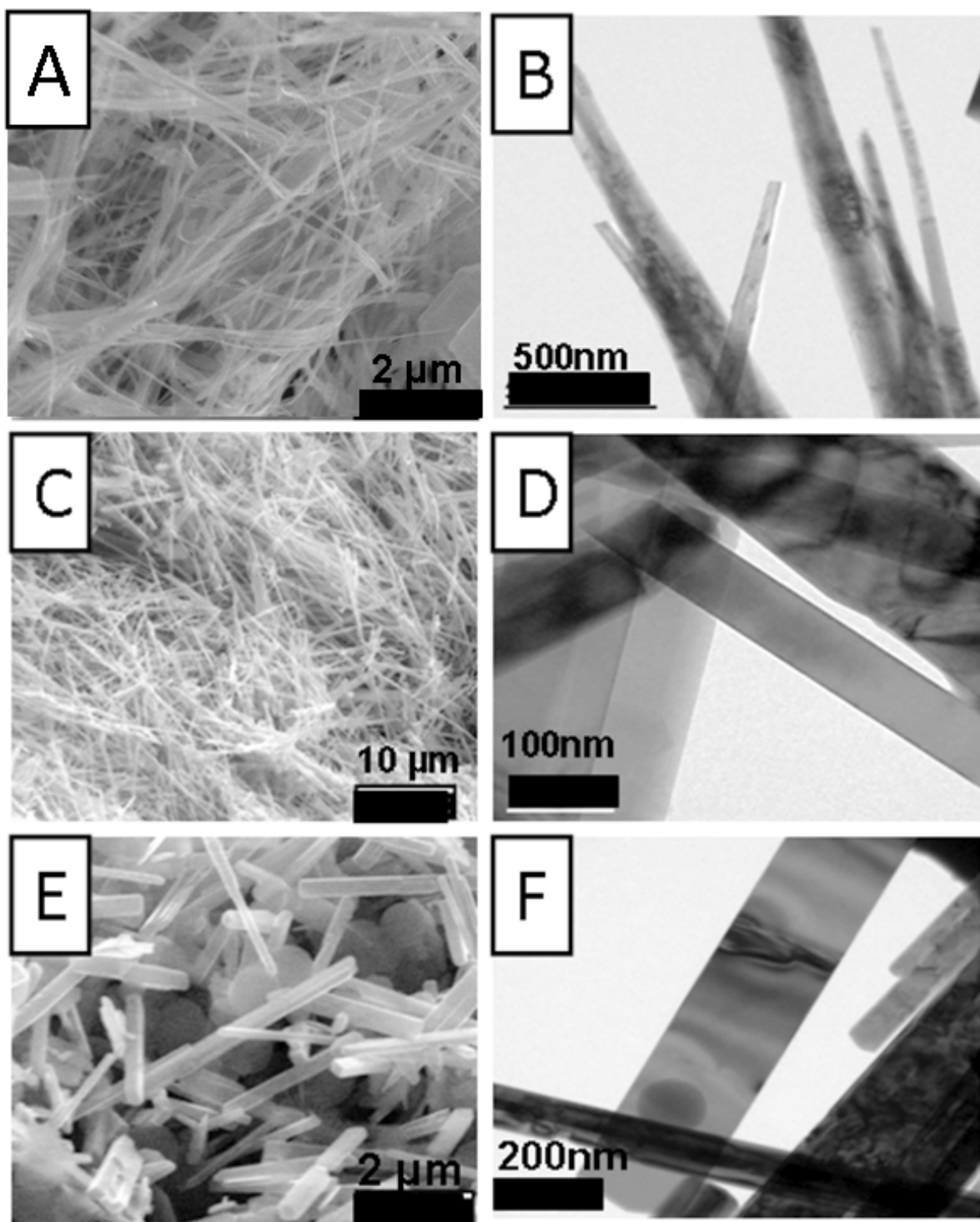
Figure 7. NEXAFS spectra acquired over a heating/cooling cycle for VO_2 nanowire samples prepared by hydrothermally treating bulk V_2O_4 with 1,3 butanediol for 7 days. The upper panel shows data upon heating at 30, 40, 60, 80, 100, and 125°C. The inset shows the changes in the satellite peak at the V L_3 edge. The lower panel shows NEXAFS spectra taken while cooling the sample from 125 to 25°C, which further corroborates the changes in the lineshapes of the π^* peak. The spectra in blue have been acquired at 30 and 25 °C, respectively, illustrating the increased hysteresis observed for the nanostructures.
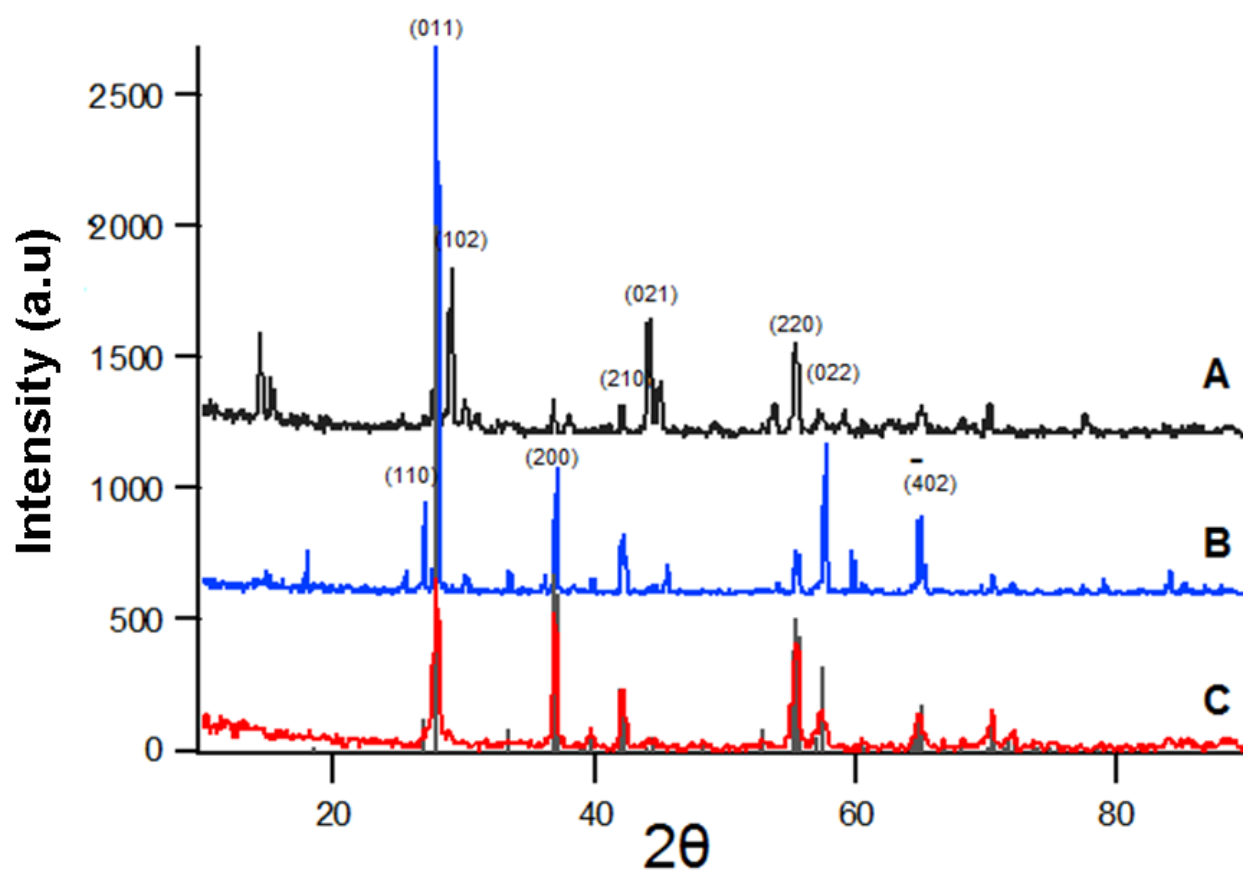
TABLES.

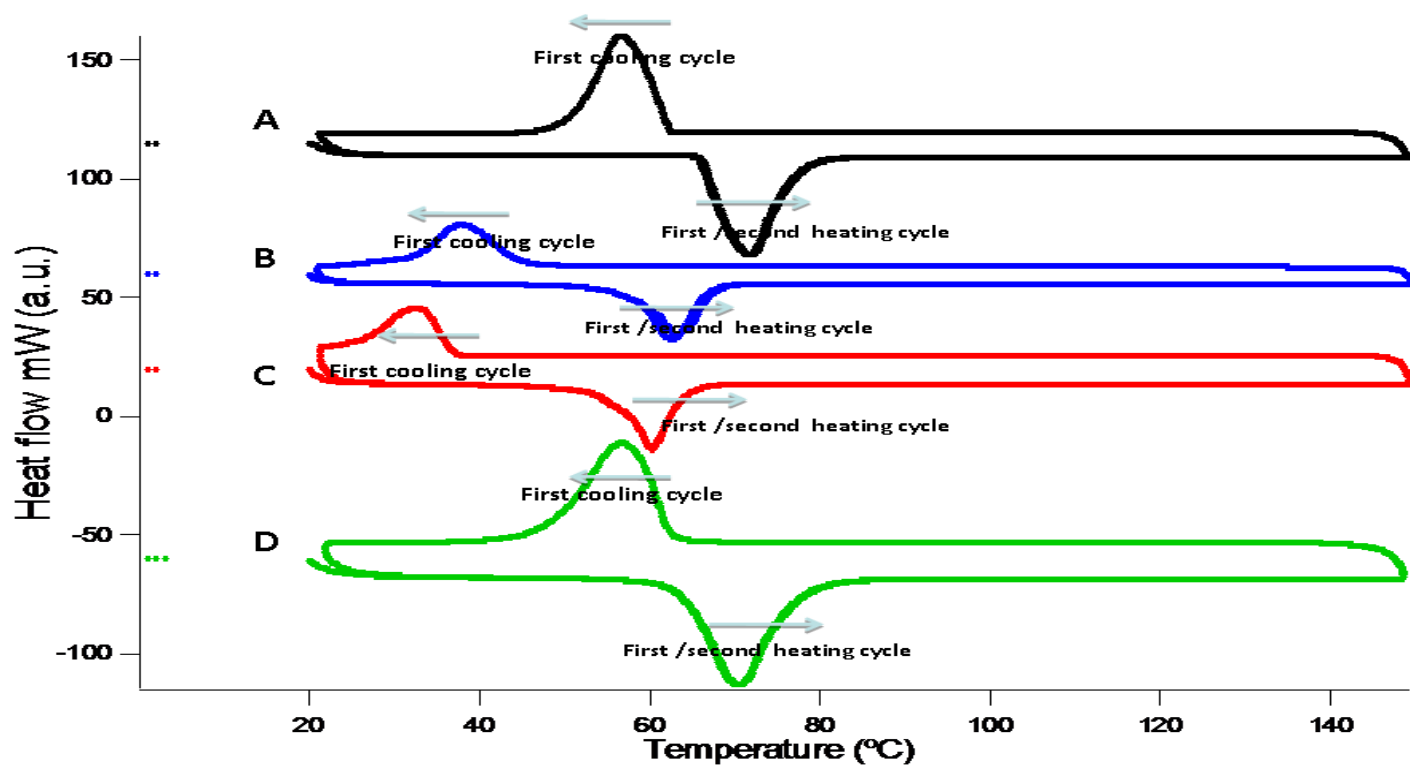**Table 1.** DSC peaks measured during cooling and heating for VO_2 nanostructures.

Figure 1. Monoclinic (distorted VO$_6$) and tetragonal (undistorted VO$_6$) polymorphs of vanadium (IV) oxide.

Figure 2. SEM (left) and TEM (right) images of VO_2 nanostructures prepared by the solvothermal reaction of bulk V_2O_4 with (A,B) 2-propanol for 3 days, (C,D) methanol for 7 days, and (E,F) 1,3 butanediol for 7 days.
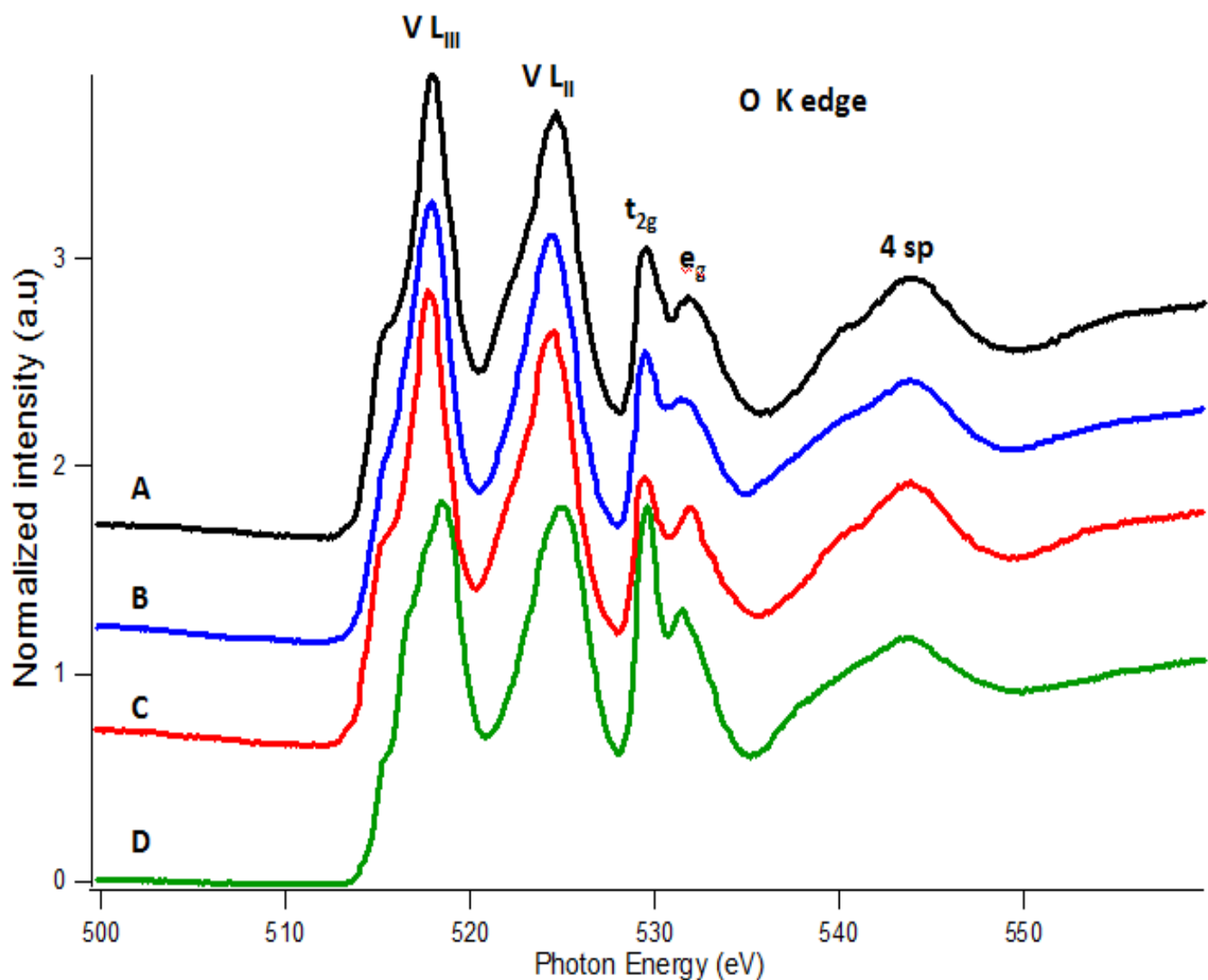
Figure 3. XRD patterns of VO_2 nanowires prepared by the hydrothermal treatment of bulk V_2O_4 with A) 2-propanol for 3 days, B) methanol for 7 days, C) 1,3 butanediol for 7 days.
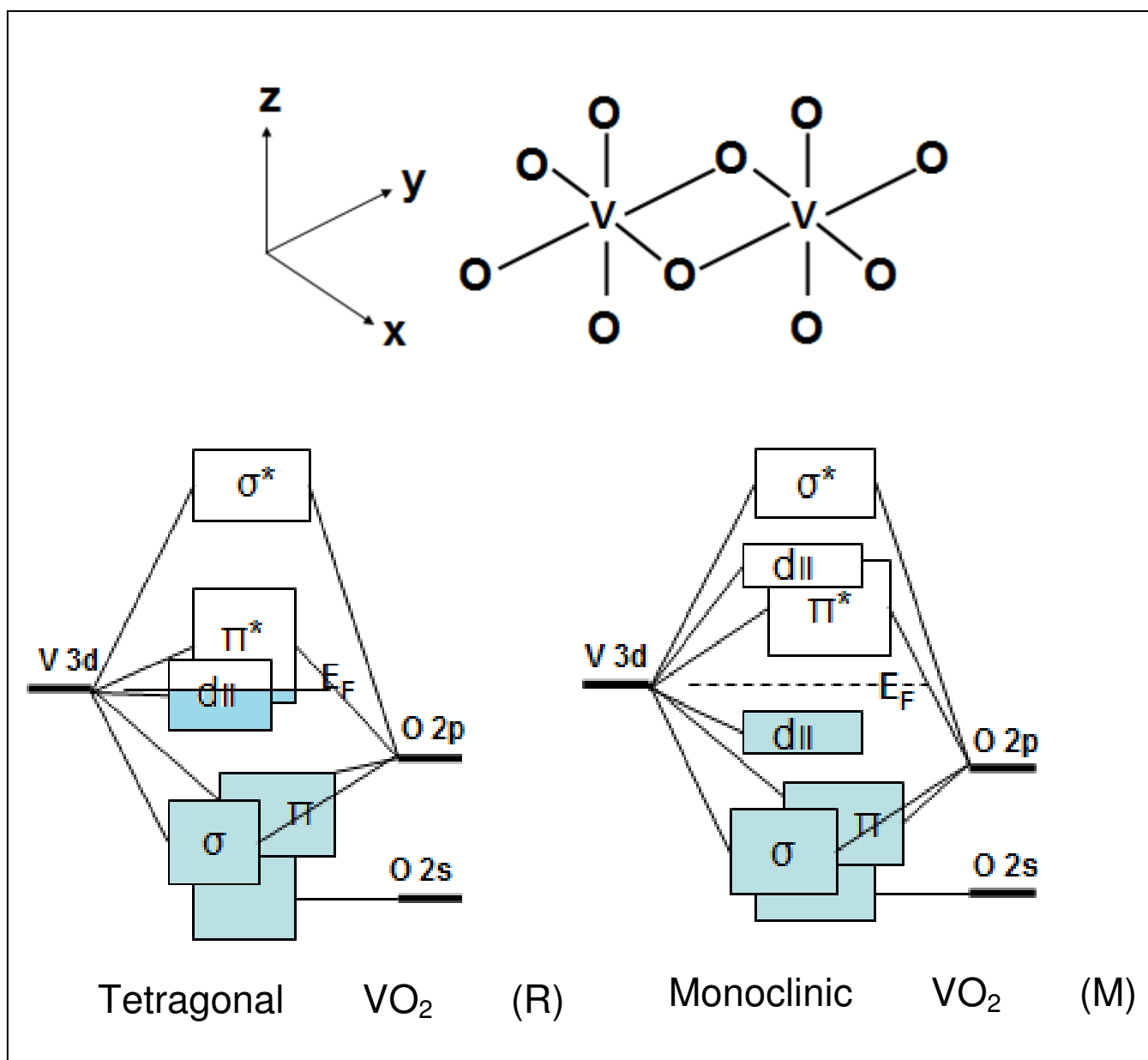
Figure 4. DSC curves obtained for VO_2 nanowires prepared by the hydrothermal treatment of bulk V_2O_4 with A) 2-propanol for 3 days, B) methanol for 7 days, and C) 1,3 butanediol for 7 days compared with the DSC trace measured for D) the bulk V_2O_4 precursor.

Structure-directing agent and reaction time	DSC temperature range 20°C to 150°C	
	Cooling peak	**Heating peak**
1,3 butanediol 7 days	32.4 °C	**60.2** °C 60.2 °C
methanol 7 days	37.9 °C	62.4 °C 63.1 °C
2-propanol 7 days	46.8 °C	**65.8** °C 66.0 °C
1,3 butanediol 3 days	57.9 °C	**69.9** °C 70.1 °C
2-propanol 3 days	56.5 °C	**71.6** °C 71.9 °C
methanol 3 days	58.9 °C	**69.6** °C 69.9 °C
octanol 3 days	57.7 °C	**70.9** °C 70.9 °C
ethanol 3 days	58.3 °C	**69.5** °C 70.5 °C
1-butanol 3 days	59.7 °C	69.6 °C 69.9 °C

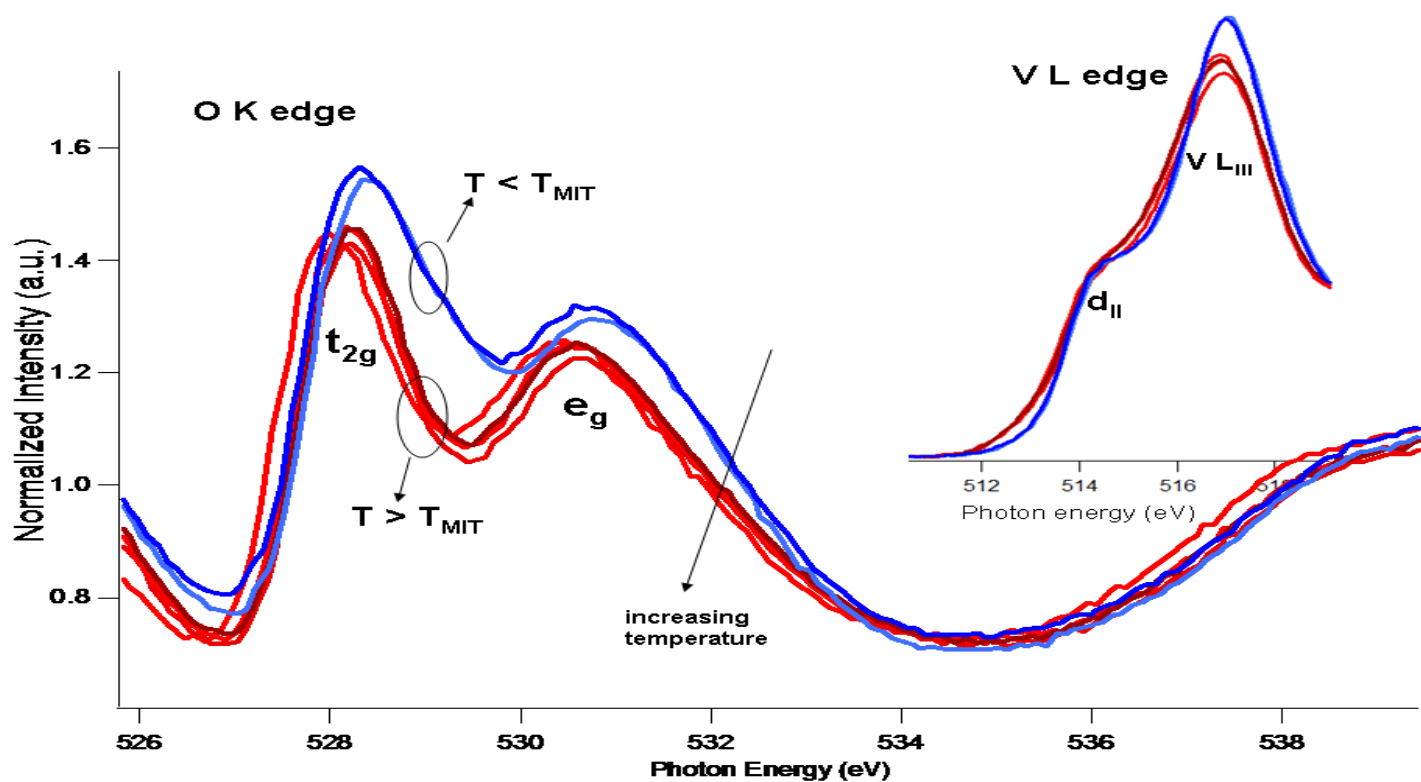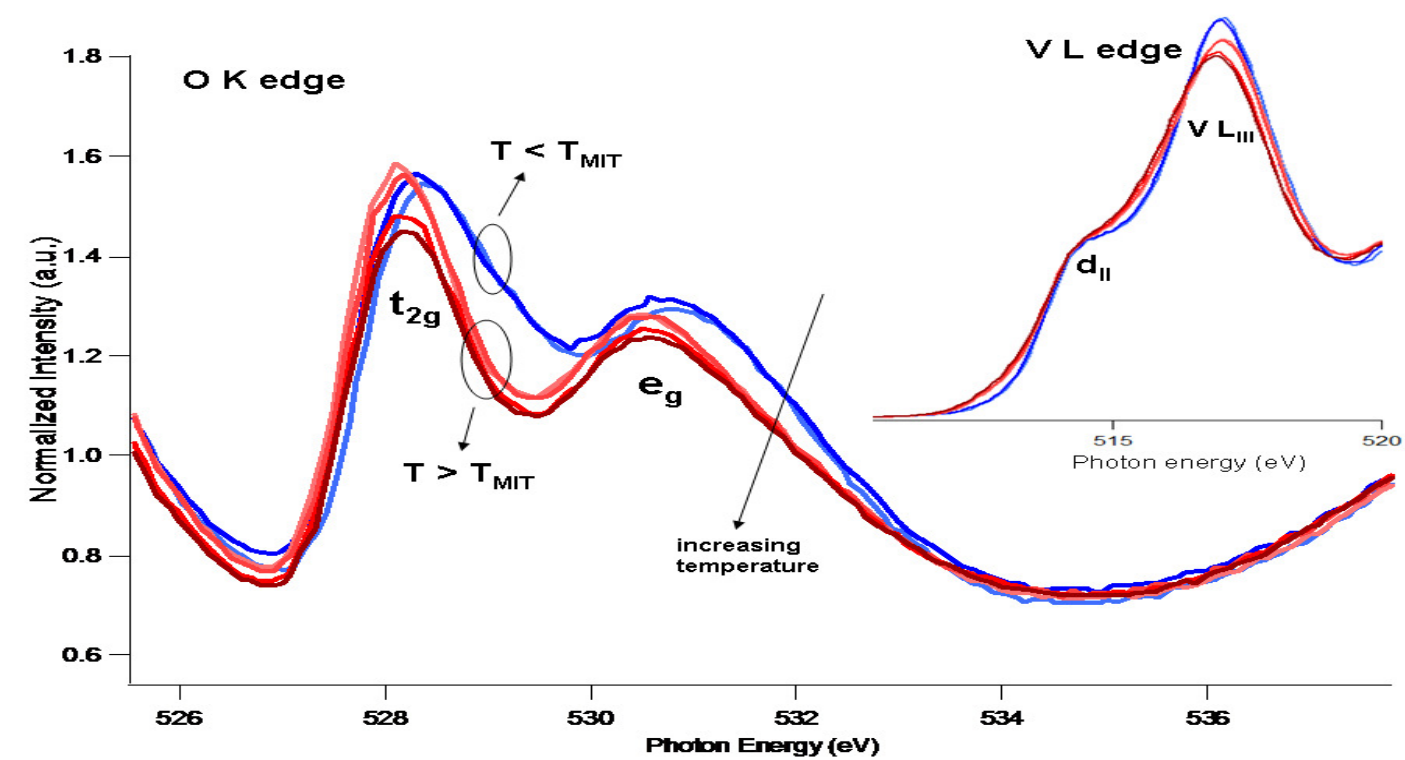**Table 1.** DSC peaks measured during cooling and heating for VO_2 nanostructures.

Figure 5. V L edge ($2p_{3/2}$, $2p_{1/2}$) and O K edge (π^*, σ^*) NEXAFS data acquired at room temperature for VO_2 nanostructures prepared by hydrothermally treating bulk V_2O_4 with A) 2-propanol for 3 days, B) methanol for 7 days, and C) 1,3 butanediol for 7 days contrasted with D) the spectra acquired for the bulk V_2O_4 powder precursor.

Figure 6. Molecular orbital diagram depicting the electronic structure of the two polymorphs of VO_2. The left MO diagram corresponds to the undistorted metallic phase of VO_2, whereas the diagram on the right shows the altered MO diagram upon transition to the distorted insulating phase of VO_2.[50]

Figure 7. NEXAFS spectra acquired over a heating/cooling cycle for VO_2 nanowire samples prepared by hydrothermally treating bulk V_2O_4 with 1,3 butanediol for 7 days. The upper panel shows data upon heating at 30, 40, 60, 80, 100, and 125°C. The inset shows the changes in the satellite peak at the V L_3 edge. The lower panel shows NEXAFS spectra taken while cooling the sample from 125 to 25°C, which further corroborates the changes in the lineshapes of the π^* peak. The spectra in blue have been acquired at 30 and 25 °C, respectively, illustrating the increased hysteresis observed for the nanostructures.
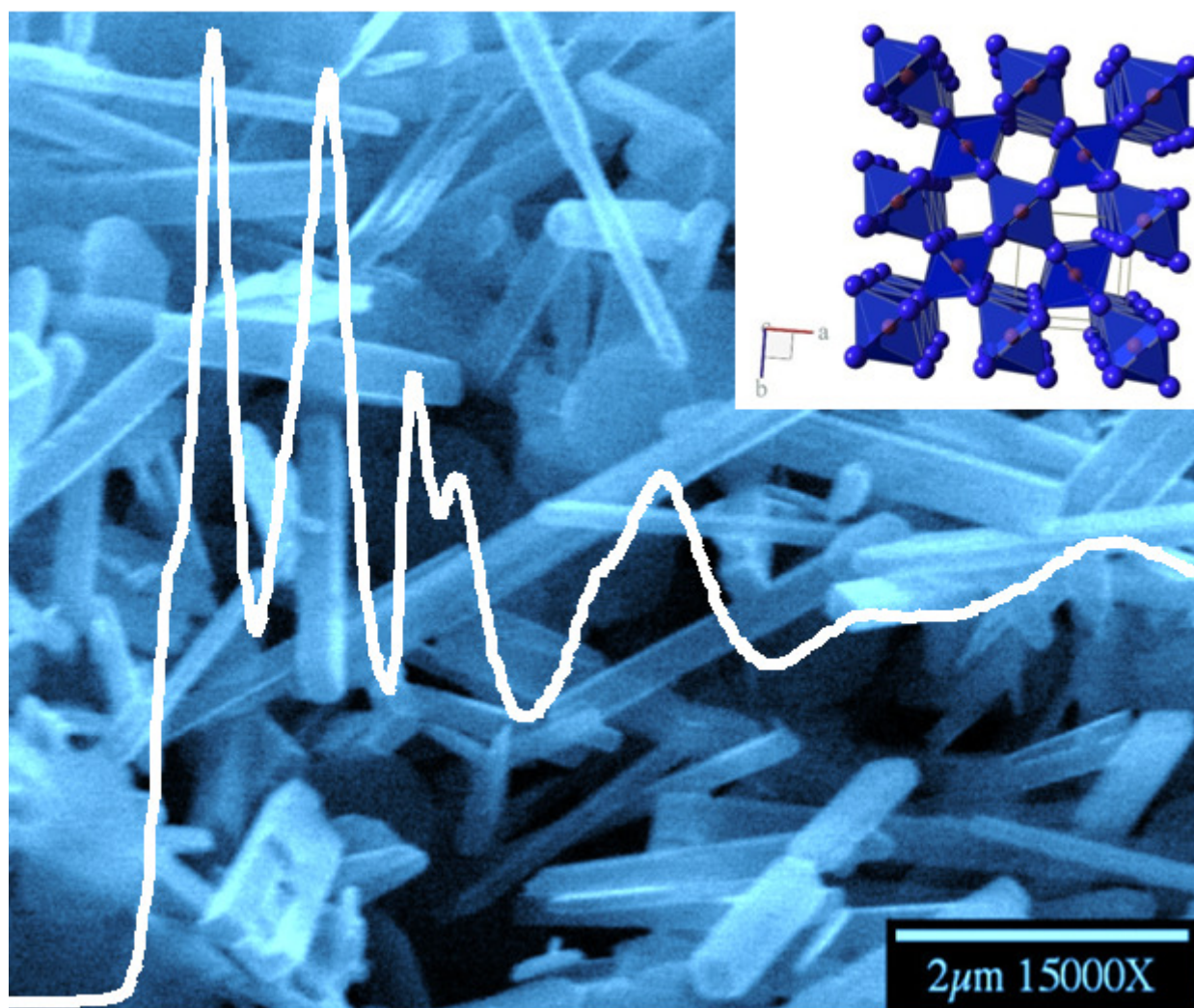
REFERENCES

1. Ozin, G. A.; Arsenault, A. C., Royal Society of Chemistry: Cambridge, UK, 2005; Vol. 1, p 594.

2. Alivisatos, A. P. *J. Phys. Chem.* **1996,** 100, 13226-13239.

3. Lieber, C. M. *MRS Bull.* **2003,** 28, 486-491.

4. El-Sayed, M. *Acc. Chem. Res.* **2004,** 37, 326-33.

5. Brus, L. E. *Appl. Phys. A* **1991,** 53, 463-474.

6. Murray, C. B.; Kagan, C. R.; Bawendi, M. G. *Annu Rev Mater Sci* **2000,** 30, 546-610.

7. Rao, C. N. R.; Raven, B., VCH: New York, 1995.

8. Law, M.; Goldberger, J.; Yang, P. *Annu. Rev. Mater. Res.* **2004,** 34, 83-122.

9. Rodriguez, J. A.; Fernandez-Garcia, M. 1st ed.; Wiley-VCH: Weinheim, 2007.

10. Surnev, S.; Ramsey, M. G.; Netzer, F. P., *Prog. Surf. Sci.* **2003,** 73, 117-165.

11. Lopez, R.; Haynes, T. E.; Boatner, L. A.; Feldman, L. C.; Haglund Jr., R. F., *Phys. Rev. B* **2002,** 65, 224113/1-224113/5.

12. Wang, Y.; Cao, G., *Chem. Mater.* **2006,** 18, 2787-2804.

13. Morin, F. J., *Phys. Rev. Lett.* **1959,** 3, 34-36.

14. Zylbersztejn, A.; Mott, N. F., *Phys. Rev. B* **1975,** 11, 4383-4395.

15. Goodenough, J. B., *J. Solid State Chem.* **1971,** 3, 490-500.

16. Winter, M.; Jurgen, O. B.; Spahr, M. E.; Novak, P., *Adv. Mater.* **1998,** 10, 725-763.

17. Lopez, R.; Boatner, L. A.; Haynes, T. E.; Feldman, L. C.; Haglund Jr., R. F., *J. Appl. Phys.* **2002,** 92, 4031-4036.

18. Lopez, R.; Feldman, L. C.; Haglund Jr., R. F., *Phys. Rev. Lett.* **2004,** 93, 177403/1-177403/4.

19. Wentzcovich, R. M.; Schulz, W. W.; Allen, P. B., *Phys. Rev. Lett.* **1994,** 72, 3389-3392.

20. Cavalleri, A.; Dekorsky, T.; Chong, H. H. W.; Kieffer, J. C.; Schoenlein, W., *Phys. Rev. B* **2004,** 70, 161102/1-161102/4.

21. Laad, M. S.; Craco, L.; Muller-Hartmann, E., *Phys. Rev. B* **2006,** 73, 195120/1-195120/7.

22. Stefanovich, G.; Perhament, A.; Stefanovich, D., *J. Phys. : Condens. Matter* **2000,** 12, 8837-8845.

23. Kim, H.-T.; Chae, B.-G.; Youn, D.-H.; Maeng, S.-L.; Kim, G.; Kang, K.-Y.; Lim, Y.-S., *New J. Phys.* **2004,** 6, 51-59.

24. Kim, H.-T.; Lee, Y. W.; Kim, B.-G.; Chae, B.-G.; Yun, S. J.; Kang, K.-Y.; Han, K. J.; Yee, K.-J.; Lim, Y.-S., *Phys. Rev. Lett.* **2006,** 2006, (266401/1-266401/3).

25. Biermann, S.; Poteryaev, A.; Lichtenstein, A. I.; Georges, A., *Phys. Rev. Lett.* **2005,** 94, 026404.

26. Koethe, T. C.; Hu, Z.; Haverkort, M.; Schubler-Langeheine, C.; Venturini, F.; Brookes, N. B.; Tjernberg, O.; Reichelt, W.; Hsieh, H. H.; Lin, H.-J.; Chen, C. T.; Tjeng, L. H., *Phys. Rev. Lett.* **2006,** 97, 116402/1-116402/4.

27. Haverkot, M.; Hu, Z.; Tanaka, A.; Reichelt, W.; Streltsov, S.; Korotin, M. A.; Anisimov, V. I.; Hsieh, H. H.; Lin, H.-J.; Chen, C. T.; Khomskii, D. I.; Tjeng, L. H., *Phys. Rev. Lett.* **2005,** 95, 196404/1-196404/4.

28. Andersson, G., I. Phase Analysis. *Acta Chem. Scand.* **1954,** 8, 1599-1606.

29. Kim, H.-T.; Chae, B.-G.; Youn, D.-H.; Kim, G.; Kang, K.-Y.; Lee, S.-J.; Kim, K.-B.; Lim, Y.-S., *Appl. Phys. Lett.* **2005,** 86, 242101/1-242101/3.

30. Kim, B.-G.; Lee, Y. W.; Choi, S.; Lim, J.-W.; Yun, S. J.; Kim, H.-T.; Shin, T.-J.; Yun, H.-S., *Phys. Rev. B* **2008,** 77, 235401/1-235401/5.

31. Boriskov, P. P.; Velichko, A. A.; Pergament, A. L.; Stefanovich, G. B.; Stefanovich, D. G., *Tech. Phys. Lett.* **2002,** 28, 406-408.

32. Maeng, J.; Kim, T.-W.; Jo, G.; Lee, T., *Mater. Res. Bull.* **2008,** 43, 1649-1656.

33. Wu, J.; Gu, Q.; Guiton, B. S.; Leon, N.; Ouyang, L.; Park, H., *Nano Lett.* **2006**, 2313.

34. Wu, X.; Tao, Y.; Dong, L.; Wang, Z.; Hu, Z., *Mater. Res. Bull.* **2005,** 40, 315-321.

35. Liu, J.; Li, Q.; Wang, T.; Yu, D.; Li, Y., *Angew. Chem. Int. Ed.* **2004,** 43, 5048-5052.

36. Barker Jr., A. S.; Verleur, H. W.; Guggenheim, H. J., *Phys. Rev. Lett.* **1966,** 17, 1286-1289.

37. Griffiths, C. H.; Eastwood, H. K., *J. Appl. Phys.* **1974,** 45, 2201-2206.

38. Ruzmetov, D.; Senanayake, S. D.; Narayanamurti, V.; Ramanathan, S., *Phys. Rev. B* **2008,** 77, 195442/1-195442/5.

39. Gui, Z.; Fan, R.; Mo, W.; Chen, X.; Yang, L.; Zhang, S.; Hu, Y.; Wang, Z.; Fan, W., *Chem. Mater.* **2002,** 14, 5053-5056.

40. Guiton, B. S.; Gu, Q.; Prieto, A. L.; Gudiksen, M. S.; Park, H., *J. Am. Chem. Soc.* **2005,** 127, 498-499.

41. Wei, M.; Sugihara, H.; Honma, I.; Ichihara, M.; Zhou, H., *Adv. Mater.* **2005,** 17, 2964-2969.

42. Sediri, F.; Touati, F.; Gharbi, N., *Materials Science and Engineering: B* **2006,** 129, (1-3), 251-255.

43. Hagrman, D.; Zubieta, J.; Warren, C. J.; Meyer, L. M.; Treacy, M. M. J.; Haushalter, R. C., *J. Solid State Chem.* **1998,** 138, 178-182.

44. Zhang, S.; Peng, L. M.; Chen, Q.; Du, G. H.; Dawson, G.; Zhou, W. Z., *Phys. Rev. Lett.* **2003,** 91, 256103/1-256103/4.

45. Schilbe, P.; Maurer, D., *Mater. Sci. Eng. A* **2004,** 370, 449-452.

46. Berglund, C. N.; Guggenheim, H. J., *Phys. Rev.* **1969,** 185, 1022-1033.

47. Salker, A. V.; Seshan, K.; Keer, H. V., *Phys. Status Solidi A* **1983,** 75, K37-K40.

48. Stohr, J., *NEXAFS Spectroscopy*. Springer: Berlin, 1992.

49. Ruzmetov, D.; Senanayake, S. D.; Ramanathan, S., *Phys. Rev. B* **2007,** 75, 195102/1-195102/7.

50. Abbate, M.; De Groot, F. M. F.; Fuggle, J. C.; Ma, Y. J.; T., C. C.; Sette, F.; Fujimori, A.; Ueda, Y.; Kosuge, K., *Phys. Rev. B* **1991,** 43, 7263-7266.

51. Chen, J. G., *Surf. Sci. Reports* **1997,** 30, 1-152.

52.   Shin, S.; Suga, S.; Taniguchi, M.; Fujisawa, M.; Kanzaki, H.; Fujimori, A.; Daimon, H.; Ueda, Y.; Kosuge, K.; Kachi, S., *Phys. Rev. B* **1990,** 41, 4993.

53.   deGroot, F. M. F.; Grioni, M.; Fuggle, J. C.; Ghijsen, J.; Sawatzky, G. A.; Peterson, H., *Phys. Rev. B* **1989,** 40, 5715-5723.

TOC